Mechanism of Cph1 Phytochrome Assembly from Stopped-Flow Kinetics and Circular Dichroism†

Berthold Borucki,‡ Harald Otto,‡ Gregor Rottwinkel,§ Jonathan Hughes,|| Maarten P. Heyn,*,‡ and Tilman Lamparter§

Biophysics Group, Department of Physics, Freie Universität Berlin, Arnimallee 14, D-14195 Berlin, Germany, Plant Physiology, Department of Biology, Freie Universität Berlin, Königin-Luise-Strasse 12, D-14195 Berlin, Germany, and Plant Physiology, Department of Biology, Justus-Liebig Universität Giessen, Senckenbergstrasse 3, D-35390 Giessen, Germany

Received August 22, 2003; Revised Manuscript Received September 23, 2003

ABSTRACT: The kinetics and mechanism of the autocatalytic assembly of holo-Cph1 phytochrome (from *Synechocystis*) from the apoprotein and the bilin chromophores phycocyanobilin (PCB) and phycoerythrobilin (PEB) were investigated by stopped flow and circular dichroism. At 1:1 stoichiometry, pH 7.9, and 10 °C, SVD analysis of the kinetic data for PCB revealed three spectral components involving three transitions with time constants $\tau_1 \sim 150$ ms, $\tau_2 \sim 2.5$ s, and $\tau_3 \sim 50$ s. τ_1 was associated with a major red shift and transfer of oscillator strength from the Soret region to the 680 nm region. When the sulfhydryl group of cysteine 259 was blocked with iodoacetamide, preventing the formation of a covalent adduct, a noncovalent red-shifted complex (680 nm) was formed with a time constant of 200 ms. τ_1 could thus be assigned to the formation of a noncovalent complex. The absorption changes during τ_1 are due to the formation of the extended conformation of the linear tetrapyrrole and to its protonation in the binding pocket. From the concentration and pH dependence of the kinetics we obtained a value of 1.5 μM for the K_D of this noncovalent complex and a value of 8.4 for the pK_a of the proton donor. The τ_2 component was associated with a blue shift of about 25 nm and was attributed to the formation of the covalent bond (P_r), accompanied with the loss of the 3−3′ double bond to ring A. τ_3 was due to photoconversion to P_{fr}. For PEB, which is not photochromic, the formation of the noncovalent complex is faster ($\tau_1 = 70$ ms), but the covalent bond formation is about 80 times slower ($\tau_2 = 200$ s) than with the natural chromophore PCB. The CD spectra of the PCB adduct in the 250−800 nm range show that the chromophore geometries in P_r and P_{fr} are similar to those in plant phytochrome. The opposite rotational strengths of P_r and P_{fr} in the longest wavelength band suggest that the photoisomerization induces a reversal of the chirality. The Cph1 complex with noncovalently bound PCB was still photochromic when cysteine 259 was blocked with IAA or with the bulkier IAF. The covalent linkage to cysteine 259 is thus not required for photoconversion. The CD spectra of the noncovalently bound PCB in P_r- and P_{fr}-like states are qualitatively similar to those of the covalent adducts, suggesting analogous structures in the binding pocket. The noncovalent interactions with the binding pocket are apparently sufficient to hold the chromophore in the appropriate geometry for photoisomerization.

Phytochromes are biliprotein photoreceptors of plants, fungi, and bacteria that allow these organisms to respond to environmental light conditions (for reviews, see refs *1*−*3*). Typical phytochromes are homodimers with each subunit consisting of an N-terminal sensor domain and a C-terminal protein kinase domain. Plant phytochromes may be regarded as light-regulated serine/threonine kinases, whereas most bacterial phytochromes including Cph1[1] from *Synechocystis* are light-regulated histidine kinases (*3*, *4*). The prosthetic groups are linear tetrapyrroles (PΦB or PCB, see Figure 1) that are covalently bound via a thioether linkage to conserved cysteine residues in 1:1 stoichiometry. Phytochromes exist in two thermostable states, the red (P_r) and far-red (P_{fr}) absorbing forms that can be reversibly switched by light (photochromism). Depending on the system either P_r or P_{fr} is the active form. Photoconversion is associated with very rapid isomerization (picoseconds) around the C_{15}═C_{16} double bond followed by a series of slower (microseconds, mil-

† This research was supported by grants from the Deutsche Forschungsgemeinschaft to M.P.H. (Sfb 498, TP B1), T.L. (Sfb 498, TP B2), and J.H. (Sfb 498,TP B2).

* To whom correspondence should be addressed: e-mail, heyn@physik.fu-berlin.de; fax, ++49-30-838-56299; phone, ++49-30-838-56160.

‡ Department of Physics, Freie Universität Berlin.

§ Department of Biology, Freie Universität Berlin.

|| Department of Biology, Justus-Liebig Universität Giessen.

[1] Abbreviations: PCB, phycocyanobilin; PEB, phycoerythrobilin; PΦB, phytochromobilin; P_r, red absorbing form of phytochrome; P_{fr}, far-red absorbing form of phytochrome; Cph1, cyanobacterial phytochrome from *Synechocystis*; Cph1Δ2, N-terminal chromophore-carrying domain of Cph1 lacking the histidine kinase domain; Rcp1, response regulator for cyanobacterial phytochrome; PAS, acronym formed from the names of the first three proteins recognized as sharing this sensory domain; CD, circular dichroism; SAR, specific absorbance ratio (ratio of the absorbance maxima in the visible region to the absorbance at 280 nm for the P_r form); IAA, iodoacetamide; IAF, iodoacetamidofluorescein; SVD, singular value decomposition.

10.1021/bi035511n CCC: $25.00
Published on Web 10/30/2003

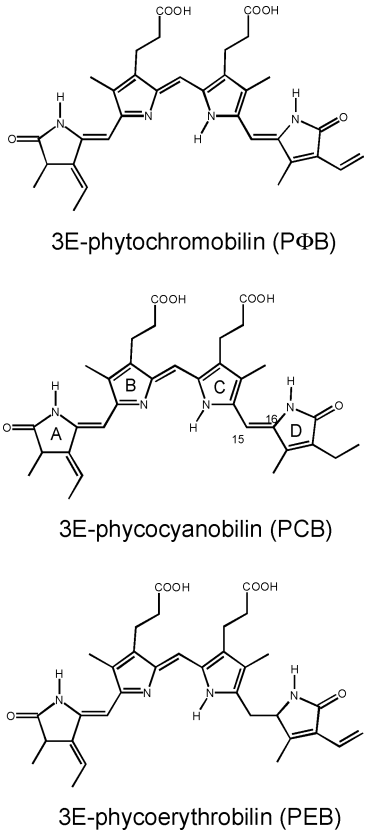

FIGURE 1: Structural formulas of the bilin chromophores PΦB, PCB, and PEB.

liseconds) conformational changes in the dark. Allosteric interactions play an important role in the activation of phytochrome. The local conformational change in the binding pocket, which is located in the sensor domain, ultimately leads to a structural change and signaling in the remote signal transduction domain. The photocycle has been studied by transient optical absorption spectroscopy (*5*, *6*) and is associated with transient proton uptake and release from the external medium (*6*). The chromophore structure in P_r, P_{fr}, and various intermediates was characterized by resonance Raman and FTIR spectroscopy (*7*−*9*). The current consensus view is that the chromophore adopts an extended ZZZ/asa configuration/conformation in P_r, which changes to ZZE/ass in P_{fr} (*10*). These studies also showed that the chromophore remains protonated throughout the photocycle (*8*, *10*). Autophosphorylation requires the homodimer structure. PAS domains are involved in the subunit−subunit interactions.

Attachment of the bilin chromophores is autocatalytic (*11*). Apophytochrome has thus also an intrinsic bilin C−S lyase activity. The mechanism of the autocatalytic assembly reaction has been studied in considerable detail (*12*). Mutants were used to identifiy residues critical for bilin attachment (*13*−*15*). Chromophore analogues were employed to determine structural determinants for proper binding (*16*, *17*). Fluorescence depolarization experiments indicate that the chromophore is highly immobilized in its binding pocket (*18*).

No high-resolution structure of phytochrome is available. Low-angle X-ray scattering data suggest an elongated prolate dimer structure (*19*). An interchromophore distance of 56 ± 7 Å in the Cph1 dimer was recently obtained from fluorescence energy transfer experiments (*18*).

The kinetics of the autoassembly of bilins and apophytochromes have been studied both in plant (*12*, *16*, *20*, *21*) and in bacterial (*22*, *23*) phytochromes using absorption in the visible or fluorescence as the signals. A very sensitive assay was introduced on the basis of the high fluorescence of the nonisomerizable bilin analogue PEB, which has a single bond at the $C_{15}-C_{16}$ position (*12*). In this pioneering study these authors proposed and analyzed a reaction scheme for the bilin binding, consisting of a rapid preequilibrium between apoprotein and bilin forming a noncovalent complex, followed by the slower irreversible formation of the covalent adduct (*12*). The time resolution of these and other studies (*22*, *23*) was limited to seconds or minutes and clearly insufficient to resolve the early steps in the kinetics.

Whereas at neutral pH the free bilin chromophores are unprotonated, there is strong evidence from vibrational spectroscopy that the bound chromophore is protonated at pH 7 in P_r in both plant (*8*, *10*) and cyanobacterial (*24*) phytochromes. As part of the assembly process the chromophore thus has to be protonated. The protonation occurs at the dipyrrin moiety of rings B and C.

The phycobiliprotein phycocyanin, which also carries PCB as the chromophore, has an absorption spectrum similar to that of the P_r form of phytochromes. Although the primary structures of both protein classes are different, the conformation and protonation state of the chromophores are thought to be comparable. From the high-resolution crystal structures of phycocyanin (*25*) and the related phycobiliproteins allophycocyanin (*26*), phycoerythrocyanin (*27*), and phycoerythrin (*28*, *29*), a common principle emerged for the protonation of their bilin chromophores. In each structure the chromophore is arched in an extended banana-shaped form around a conserved aspartate residue with the N atoms of pyrroles B and C within hydrogen-bonding distance of one of the carboxylate oxygens. The positive charge of the protonated bilin is delocalized between the two nitrogens and balanced by the negative charge of the aspartate. The formation of this ion pair in biliproteins requires a precise position and orientation of the chromophore in its binding pocket. It is likely that the carboxyl group of this aspartic acid residue also serves as the internal proton donor in the chromophore protonation. Although no high-resolution structure is available for phytochrome, it is plausible that a similar ion pair formation is an essential step in its assembly as well. In fact, for Cph1 it was observed that no assembly occurs when E189 is substituted by A, G, K, and T, suggesting that the carboxyl group of glutamate 189 may serve this role as the proton donor (*15*) or that it is essential for proper folding. Studies with a model compound, which is the adduct of cysteine and phycocyanobilin dimethyl ester, showed that intramolecular proton transfer to the chromophore leads to a large red shift of about 60 nm and an approximately 3-fold increase in oscillator strength of the longest wavelength transition (*30*). Intramolecular protonation of the phytochrome chromophore is thus expected to lead to a significant bathochromic shift which should be observable if the assembly kinetics are monitored by UV−vis absorbance spectroscopy.

The formation of the covalent bond, on the other hand, is expected to cause a spectral blue shift since the 3−3′ double bond is lost in the process, leading to a smaller conjugated

π-system. Additional noncovalent interactions between the chromophore and binding pocket which might contribute to the proper orientation and anchoring of the bilin involve the two negatively charged propionate side chains of rings B and C. Methylation of both carboxyl groups abolished ligation, suggesting that the electrostatic interaction of these negatively charged groups with corresponding positive charges of the protein is required for autoassembly (*17*). Hydrogen bonds between NH groups of the rings and acceptor groups in the binding pocket provide further noncovalent interactions.

Since intramolecular proton transfer and formation of a salt bridge (ion pair) would seem to be a prerequisite for the formation of the covalent bond, a working model of the assembly mechanism would consist of the following steps: (1) rapid reversible noncovalent association with the chromophore in an extended conformation in the binding pocket (this reaction could be diffusion controlled); (2) intramolecular proton transfer from an internal donor inside the binding pocket and formation of an ion pair and hydrogen bonds; (3) irreversible formation of the covalent bond. Since each of these steps is expected to be associated with absorbance changes, they may lead to kinetically observable signals.

Here, we study the assembly kinetics and mechanism in the cyanobacterial phytochrome Cph1 from *Synechocystis* (*4*, *31*, *32*) with PCB, the natural chromophore of Cph1 (*33*), and PEB. Cph1 has a lower molecular mass than plant phytochrome (85 vs 124 kDa), since it lacks the ~300-residue PAS domain. We used the stopped-flow method (1) for a quantitative analysis of the assembly kinetics in vitro and (2) for improved time resolution. The availability of large amounts of apo-Cph1, expressed in *Escherichia coli*, allow such experiments for the first time. Using a CCD array for detection, complete transient absorption spectra from 300 to 800 nm were recorded with a time resolution of 10 ms. The broad bandwidth allowed a spectral characterization of the assembly intermediates.

MATERIALS AND METHODS

Expression and Purification of Cph1. Full-length Cph1 (*Synechocystis* phytochrome, gene *slr0473* from strain PCC6803) was expressed in *E. coli* with a C-terminal histidine tag and purified as described (*22*).

Bilin Chromophores. PCB and PEB were extracted and purified as described (*22*).

Stopped-Flow Setup and Measurements. The apparatus consists of a thermostated stopped-flow mixing unit (SHU-61; Hi-Tech, Salisbury, U.K.) with a dead time of less than 2 ms and a home-built detection part. The observation cell of the mixing unit (path length 10 mm) is connected with fiberoptic light guides to a 75 W Xe light source (XBO 75; Müller Elektronik-Optik, Moosinning, Germany) and to a 125 mm spectrometer (77400-M; Oriel Instruments, Stratford, CT). A linear CCD array (CCD2010; Entwicklungsbüro G. Stresing, Berlin, Germany) attached to the spectrometer allows multiple wavelength detection at 512 wavelength points. The intensity of the light source was reduced appropriately to operate the CCD array at the highest sensitivity. The assembly was initiated by mixing equal volumes (each about 100 μL) of solutions of apoprotein and bilin chromophore, both at the same buffer concentration (50 mM Tris, 5 mM EDTA) and the same pH value. Complete spectra $I(\lambda,t)$ were taken at 20000 discrete time points after mixing, typically from 10 ms to 200 s. The data were averaged to 60 wavelength points (about 8 nm spaced) and to 59 time points which are regularly distributed on a logarithmic time scale. A reference spectrum without the absorbing species $I_R(\lambda)$ (i.e., with water only) was acquired to calculate the transient absorption $A(\lambda,t)$ as an absolute property: $A(\lambda,t) = \log[I_R(\lambda)/I(\lambda,t)]$. The wavelength scale of the absorption spectra was calibrated by comparison with the steady-state absorption spectra from the spectrophotometer (UV-260; Shimadzu, Japan). To investigate the kinetics of the P_r to P_{fr} photoconversion due to the measuring light without interference from the assembly process, holophytochrome was converted to the P_r state by far-red light irradiation and then transferred to the observation cell by stopped-flow mixing.

Analysis of the Stopped-Flow Data. The transient absorbance changes with respect to the final state at 200 s were calculated according to $\Delta A(\lambda,t) = \log[I(\lambda,200\text{ s})/I(\lambda,t)]$. Using a matrix representation of $\Delta A(\lambda,t)$ a singular value decomposition (SVD) was carried out:

$$\Delta\mathbf{A} = \mathbf{U}^{\mathrm{T}}\mathbf{D}(s)\mathbf{V} \tag{1}$$

The time traces of the relevant SVD components $V_i(t)$ weighted with the related SVs s_i were fitted simultaneously with a sum of exponentials:

$$s_i V_i(t) = G_{i0} + \sum_j G_{ij} \mathrm{e}^{-t/\tau_j} \tag{2}$$

From the amplitudes G_{ij} of this fit and the basis spectra U_i the amplitude spectra B_j were calculated:

$$B_j(\lambda) = \sum_i U_i(\lambda) G_{ij} \Leftrightarrow \mathbf{B} = \mathbf{U}^{\mathrm{T}}\mathbf{G} \tag{3}$$

To determine the spectra and the time courses of the species involved, the data of the photoconversion experiment were included by performing a joint SVD of both the assembly and the photoconversion data (subscripts a and p, respectively).

$$(\Delta\mathbf{A}_a, \Delta\mathbf{A}_p) = \mathbf{U}^{\mathrm{T}}\mathbf{D}(s)(\mathbf{V}_a, \mathbf{V}_p) \tag{4}$$

A linear transformation $\mathbf{X}^{-1}$ provides the difference spectra between the pure species $\vec{A}_i$ ($i = 1, ..., n$) and the final state at 200 s after mixing $\vec{A}_f$ in the assembly process:

$$\vec{A}_i - \vec{A}_f = \mathbf{U}^{\mathrm{T}}(\mathbf{X}^{-1})_i \tag{5}$$

The transformation matrix $\mathbf{X}^{-1}$, on the other hand, results from specific assumptions on the above difference spectra by inversion of eq 5. Since $\mathbf{X}^{-1}$ is not a square matrix ($n - 1$ basis spectra are transformed in the spectra of n species), the transformation of the time traces $\mathbf{V}_a$ with $\mathbf{X}$ ($\mathbf{n}_a = \mathbf{X}\mathbf{V}_a$) fails. Instead, the time traces of the pure species have to be calculated from the transient absorption spectra $\mathbf{A}_a$ and the absorption spectra of the pure species $\mathbf{A}_S = (\vec{A}_1, ..., \vec{A}_n)$.

$$\mathbf{n}_a = \mathbf{A}_S{}^{-1}\mathbf{A}_a \tag{6}$$

In the first step of the assembly a noncovalent complex (P + C ⇌ P•C) is formed. The stationary concentration of the complex [P•C] is given by

$$[\mathrm{P{\cdot}C}] = c_\mathrm{p}\left(\frac{1 + c_\mathrm{c}/c_\mathrm{p} + K_\mathrm{D}/c_\mathrm{p}}{2} - \sqrt{\left(\frac{1 + c_\mathrm{c}/c_\mathrm{p} + K_\mathrm{D}/c_\mathrm{p}}{2}\right)^2 - c_\mathrm{c}/c_\mathrm{p}}\right) \quad (7)$$

with c_c and c_p the total concentrations of C (the chromophore) and P (the protein), respectively, and K_D the dissociation constant.

Circular Dichroism Experiments. Circular dichroism spectra were recorded with a Jasco 500-A instrument. The data acquisition system was upgraded with a home-built control unit and a fast A/D converter. Data were collected at room temperature, with cells of 10 mm path length, and averaged over 5−10 scans. For baseline corrections the spectra were recorded with the same cell filled with buffer.

RESULTS

Kinetics and Spectral Changes of the Stoichiometric Assembly with PCB. The assembly of the Cph1 apoprotein with its native chromophore PCB was investigated at pH 7.9 and 10 °C with equal concentrations of the apoprotein and PCB ("stoichiometric" conditions). The transmitted intensity after rapid mixing of the two solutions was measured from 10 ms to 200 s. Using a steady-state reference spectrum of pure water, the absorbance spectra were calculated for 59 time points regularly spaced on a logarithmic time scale. These absorbance spectra (average of 15 mixing experiments) are shown in a 3D representation in Figure 2A, which clearly shows a decrease in the Soret band region (around 350 nm) and an increase in the Q-bands (around 650 nm) with time. To resolve the distinct changes especially in the Q-bands, the absorbance spectra at four characteristic time delays after mixing are plotted in Figure 2B, together with a spectrum of the PCB solution mixed with buffer instead of apoprotein. Apart from a constant offset, the shape of the spectrum at 10 ms after mixing (—) is somewhat broader compared to the spectrum of the free chromophore (−×−). The continual decrease of the Soret band absorption is evident in the transient spectra from 10 ms to 200 s. The spectrum at 800 ms after mixing (---) displays an increase and a red shift in the Q-bands. The following relaxation is associated not only with a further increase of the absorption of the Q-bands but also with a blue shift of these bands, as indicated in the spectrum at 15 s after mixing (•••). The spectrum at 200 s after mixing (− + −) shows a decrease at about 650 nm and an increase in the longer wavelength region, suggesting the formation of P_{fr} in a photoequilibrium state (P_r/P_{fr}) by the measuring light. This is supported by the corresponding red shift in the Soret bands. Further evidence for this interpretation is that the rate for this reaction increases with the intensity of the measuring beam.

For a quantitative analysis we use the absorbance changes with respect to the final state at 200 s [$\Delta A(\lambda,t) = \log[I(\lambda,200\ \mathrm{s})/I(\lambda,t)]$], which does not require a reference spectrum from an independent experiment. In this way, systematic spectral artifacts from the CCD detection are reduced. The SVD analysis (eq 1) of the absorbance changes exhibits only three relevant spectral components. In a logarithmic plot of the SVs (Figure 3A), only three SVs are well above the noise level, which is indicated by the solid line. Singular values four and five are more than 10 times smaller than s_3 and only slightly above the noise level. They were neglected due to their very small amplitudes. The time traces weighted with the associated SVs [**D**(*s*)**V**] and the basis spectra (**U**) of the relevant components are shown in panels B and C of Figure 3, respectively. The traces of Figure 3B suggest (at least) three transitions and were thus fitted simultaneously with three exponentials according to eq 2. The time constants obtained in this way ($\tau_1 = 150$ ms, $\tau_2 = 2.5$ s, $\tau_3 = 56$ s) are marked by vertical dashed lines. From the amplitudes of this fit and the basis spectra the amplitude spectra B_i were calculated according to eq 3 and plotted in Figure 3D. In the case of a linear sequential mechanism, the B_i spectra have a simple interpretation as difference spectra between the sequential species. This assumption will be made. The first amplitude spectrum B_1 (■) associated with τ_1 indicates the formation of an intermediate with a λ_{max} value of about 680 nm, i.e., red shifted with respect to the λ_{max} of P_r at 655 nm. The positive amplitude at 700 nm and the negative amplitude at 650 nm in B_2 (○) imply a blue shift in this relaxation component. The negative amplitude at about 725 nm in B_3 suggests the formation of P_{fr} during the third

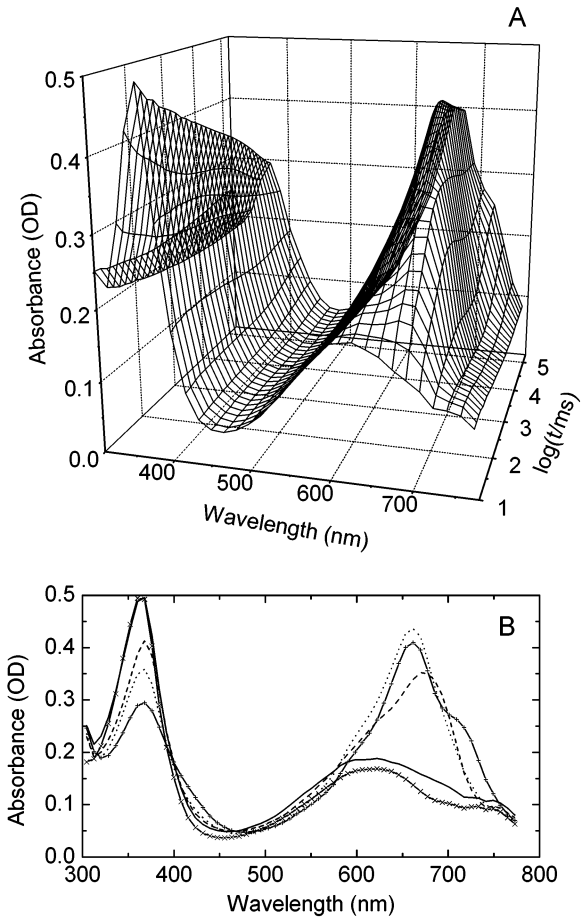

FIGURE 2: Stoichiometric assembly of apo-Cph1 with PCB at pH 7.9 and 10 °C in the time range from 10 ms to 200 s. (A) 3D representation of the absorbance as a function of wavelength and time after mixing. (B) Absorption spectra at 10 ms (—), 800 ms (---), 15 s (•••), and 200 s (−+−) and absorption spectrum of free PCB (−×−). Final holoprotein concentration = 9 μM.

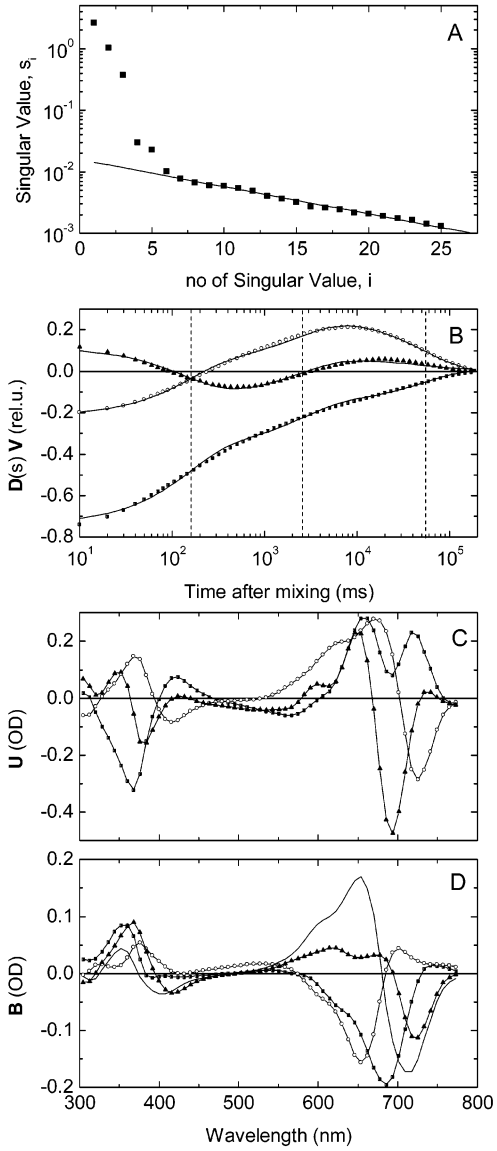

FIGURE 3: Analysis of the data of Figure 2. (A) Singular values. (B) Time traces $\mathbf{D}(s)\mathbf{V}$ of the main components of the SVD: $s_1 = 2.627$ (■), $s_2 = 0.396\ s_1$ (○), and $s_3 = 0.142\ s_1$ (▲). Solid lines represent a simultaneous fit to the data with three exponentials. Dashed vertical lines mark the time constants of the fit ($\tau_1 = 150$ ms, $\tau_2 = 2.5$ s, $\tau_3 = 56$ s). (C) SVD basis spectra. (D) Amplitude spectra calculated from the fit amplitudes of panel B and the SVD basis spectra of panel C: B_1 (■), B_2 (○), and B_3 (▲). The solid line is the $P_r - P_{fr}$ difference spectrum from the stopped-flow photoconversion experiment.

relaxation. However, the shape of B_3, especially the small amplitude at about 650 nm, differs somewhat from a typical P_r minus P_{fr} difference spectrum. As a control experiment, we studied under the same conditions the effect of the measuring light on holo-Cph1 which was initially converted to the P_r state and then quasi instantaneously exposed to the measuring light by stopped-flow transfer in the observation cell. In this case, only one spectral component was observed which displays the well-known features of a P_r minus P_{fr} difference spectrum (solid line in Figure 3D). The time constant of the relaxation was 25 s, i.e., clearly smaller than τ_3 in the assembly experiment. In all experiments τ_3 increased with increasing PCB concentration (Table 1). This is only an apparent increase, caused by the inner filter effect from excess PCB. At higher PCB concentration it takes longer

Table 1: SVD and Kinetic Analysis of the Assembly of the Cph1 Apoprotein with PCB at Different Stoichiometries

		singular values			time constants		
sample[a]	stoichiometry	s_1	s_2/s_1	s_3/s_1	τ_1/ms	τ_2/s	τ_3/s
Cph1[a]	1:0.4	0.798	0.551	0.164	203	4.7	42
	1:1	2.643	0.240	0.103	229	4.1	71
	1:2	2.508	0.280	0.138	192	4.4	93
	1:4	2.459	0.305	0.164	176	4.3	106
Cph1[b]	1:0.29	0.624	0.865	0.252	141	3.1	30
	1:0.81	2.227	0.469	0.154	155	2.5	53
	1:1	2.627	0.396	0.142	150	2.5	56
Cph1Δ2	1:0.23	0.487	0.856	0.259	131	5.3	34
	1:0.75	2.394	0.455	0.169	155	6.0	58
	1:1.5	3.685	0.306	0.144	139	5.0	86
	1:3	3.273	0.401	0.198	140	6.3	66

[a] Cph1[a] and Cph1[b] are different preparations of the full-length apoprotein. Concentrations of the apoprotein were 7.2, 9, and 7.5 μM for Cph1[a], Cph1[b], and Cph1Δ2, respectively.

for the conversion due to the decreased light intensity at the end of the cuvette. It should be mentioned that the ratios of the SVs and the values of the time constants differ somewhat between different preparations of the Cph1 apoprotein (see Table 1). However, within the same preparation the results were quite reproducible.

So far, the data analysis was model independent (B_i spectra). To make further progress and to determine the spectra and the time courses of the species involved in the assembly of apo-Cph1 with PCB, we made the following two assumptions: (1) The first relaxation reflects an equilibration between a species spectrally very similar to the free chromophore and a red-shifted intermediate. (2) The two species which appear in the second and third relaxations, respectively, and which are required to satisfy a three-step relaxation cascade are P_r and P_{fr}. The absorption spectra of the first two intermediates were calculated using assumption 1 in the following way. First, we use eq 7 to calculate the percentage of molecules in equilibrium in the red-shifted intermediate. For the dissociation constant K_D of the noncovalent equilibrium we used 1.5 μM (as determined below), and for c_p we have 9 μM. In this way we find that 67% of apo-Cph1 binds PCB and forms the red-shifted intermediate. Since this intermediate is formed with a time constant of 150 ms, we calculate that, at 10 and 200 ms, 4.3% and 49%, respectively, of the Cph1 molecules are in the red-shifted form. Since the observed absorption spectra at these two time points are linear combinations of the spectra of the first two intermediates, their spectra were obtained by inverting the corresponding linear equations.

The absorption spectra of P_r and P_{fr} were determined from the stopped-flow photoconversion experiment with holo-Cph1 (see above). These four intermediate spectra were "refined" by using a representation with the three relevant basis spectra determined from a joint SVD of the assembly and the photoconversion data according to eq 4. This "refinement" was performed in the following way. First, the transformation matrix $\mathbf{X}^{-1}$ was determined from the initial intermediate spectra $\vec{A}_i$ by inversion of eq 5, and second, the intermediate spectra were recalculated according to eq 5. The result of this procedure is shown in Figure 4A. In the transition from the first intermediate (or free chromophore) to the red-shifted intermediate and from the red-shifted intermediate to the P_r state, oscillator strength is transferred

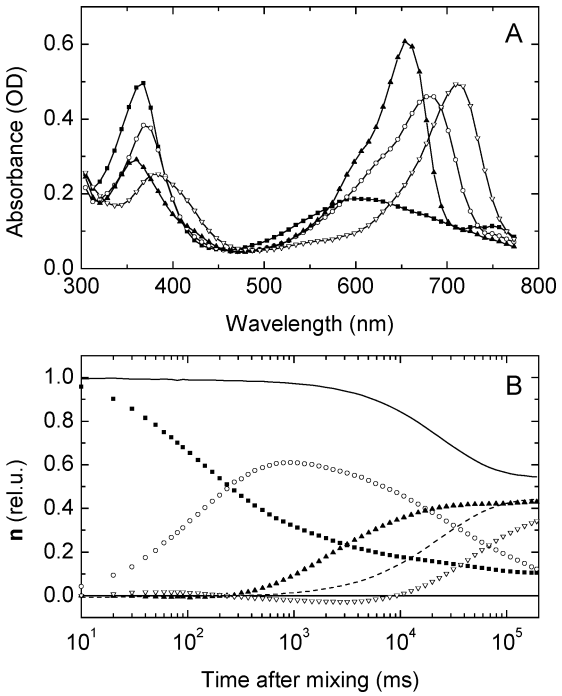

FIGURE 4: Results from the data of Figure 2 (assembly) and the photoconversion data of holo-Cph1 assuming three apparent relaxations in the assembly process. For details see text. (A) Intermediate spectra. (B) Time courses of the relative concentrations of the intermediates: first intermediate (■), red-shifted intermediate (○), P_r (▲), and P_{fr} (▽). Lines in panel B: time courses of P_r (—) and P_{fr} (---), respectively, in the photoconversion of holo-Cph1 induced by the measuring light after rapid mixing of P_r with itself.

from the Soret band to the Q-bands. The λ_{max} of the main absorption band of the red-shifted intermediate is at about 680 nm, and the Soret band is red shifted as well with respect to the P_r state. The time courses of the four species shown in Figure 4B (symbols) were calculated from the transient absorbance and the intermediate spectra according to eq 6. In the first relaxation component ($\tau_1 = 150$ ms) an equilibrium between the first intermediate (■) and the red-shifted intermediate (○) is formed. The decay of this equilibrium is associated with the second and the third relaxation component and is thus at least biphasic. The formation of the P_r (▲) and P_{fr} (▽) states occurs with the second ($\tau_2 = 2.5$ s) and third ($\tau_3 = 56$ s) relaxation, respectively. The concentration of P_r is almost constant during the third relaxation, implying that the decay of P_r due to the photoconversion is compensated by the formation of additional P_r from the red-shifted intermediate. Comparison with the photoconversion experiment with holo-Cph1 (lines in Figure 4B) indicates that the apparent formation of the P_{fr} state is retarded in the assembly measurement (56 vs 25 s).

Assembly with PCB at Different Stoichiometries. The assembly kinetics of the Cph1 apoprotein with excess PCB did not differ significantly from the stoichiometric case. For 1:2 and 1:4 stoichiometry the three relevant SVs are very similar (see Table 1), and the related time traces **D**(*s*)**V** display the same behavior (data not shown) as for the 1:1 stoichiometry. The fit of the time traces with three exponentials reveals nearly the same time constants (see Table 1), except for the third, which increases systematically with increasing PCB concentration. The time constants for the substoichiometric assembly (1:0.3 and 1:0.4) are also very

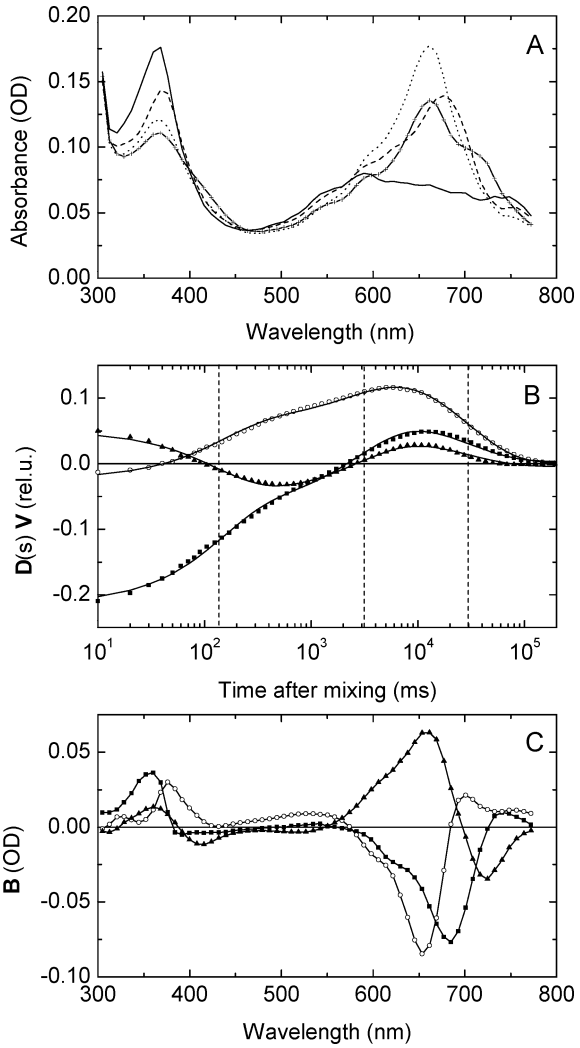

FIGURE 5: Substoichiometric assembly of apo-Cph1 with PCB ([apo]/[PCB] ~ 1:0.23) at pH 7.9 and 10 °C in the time range from 10 ms to 200 s. (A) Absorption spectra at 10 ms (—), 500 ms (---), 8 s (•••), and 200 s (− + −). (B) Time traces **D**(*s*)**V** of the main components of the SVD: $s_1 = 0.624$ (■), $s_2 = 0.865\ s_1$ (○), and $s_3 = 0.252\ s_1$ (▲). Solid lines represent a simultaneous fit to the data with three exponentials. Dashed vertical lines mark the time constants of the fit ($\tau_1 = 140$ ms, $\tau_2 = 3.1$ s, $\tau_3 = 30$ s). (C) Amplitude spectra calculated from the fit amplitudes of panel B and the SVD basis spectra (data not shown): B_1 (■), B_2 (○), and B_3 (▲).

similar (see Table 1), but the evolution of the absorption after mixing shows a considerable difference in the late time range (see Figure 5A). The absorbance decrease around 650 nm in the third relaxation, from 8 s (•••) to 200 s (− + −), is much more pronounced under these conditions (compare with Figure 2B). The SVD confirms qualitative differences in the substoichiometric assembly: The relative contribution of the second component is clearly higher ($s_2/s_1 = 0.865$ vs 0.396 for 1:1 stoichiometry; see Table 1), and the trace of the first component shows a reversal, in contrast to the monotonic behavior in the stoichiometric assembly [compare trace (■) in Figures 3B and 5B]. Consequently, the amplitude spectra of the substoichiometric assembly, shown in Figure 5C, display the following features in comparison to the amplitude spectra of Figure 3D: (a) B_2 is scaled up by about 30% with respect to B_1, (b) the negative band of B_3 at about 725 nm is slightly reduced with respect to B_1, while the

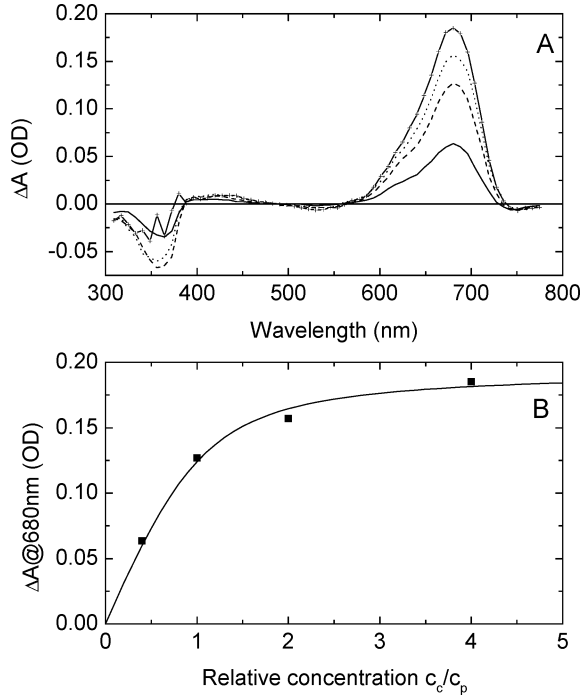

FIGURE 6: Dependence of the assembly on the concentration ratio of [apo]/[PCB]. (A) Difference spectra [A(800 ms) − A(10 ms)] at four ratios of [apo]/[PCB]: 1:0.4 (—), 1:1 (---), 1:2 (···), and 1:4 (− + −). (B) Absorbance change at 680 nm as a function of the relative concentration c_c/c_p = [PCB]/[apo]. The solid line is a fit to the data with eq 7 leading to a dissociation constant of $K_D = 1.5$ μM for the apoprotein concentration of $c_p = 7.2$ μM.

positive band at about 655 nm is strongly enhanced. The overall shape of B_3 in the substoichiometric assembly resembles the P_r minus P_{fr} difference spectrum better than in the stoichiometric case. However, the positive band in B_3 which refers to the decay of the P_r state is still too large.

According to our working hypothesis for the assembly mechanism, the first relaxation component reflects the formation of a noncovalent red-shifted complex of the chromophore with the apoprotein. It is therefore expected that the amplitude of this component displays a characteristic dependence on the concentration of the chromophore at a fixed concentration of the protein. In Figure 6A we show the difference spectrum $\Delta A = A$(800 ms) − A(10 ms) at four relative chromophore concentrations c_c/c_p. The positive band at about 680 nm shows a systematic trend, while the negative band at about 350 nm suffers from saturation effects at the high chromophore concentrations. In Figure 6B the absorbance change at 680 nm was plotted as a function of the relative chromophore concentration. The data points were fitted to eq 7 for the association equilibrium with an apparent dissociation constant of about $K_D = 1.5 \pm 0.5$ μM. While the amplitude of the first relaxation component is thus consistent with the above hypothesis, the time constant of this process does not show a significant dependence on the PCB concentration (Table 1). We note that our data satisfactorily fit to exponentials, while the kinetics of a bimolecular reaction at 1:1 stoichiometry deviates considerably from exponential behavior. Simulations of a bimolecular reaction with a K_D of 1.5 μM and at the given protein concentration revealed an expected 3-fold increase of the apparent rate constant from 1:1 to 1:4 stoichiometry. Such an acceleration was clearly not observed in our experiments, which are thus inconsistent with the proposed model. This discrepancy led us to introduce an earlier intermediate whose rapid formation is unresolved.

Experiments with the deletion mutant Cph1Δ2, which lacks the C-terminal histidine kinase domain, led to nearly the same results as with the full-length protein (see Table 1). The SVD revealed as well three spectral components involving a three-step relaxation process. As for full-length Cph1, at low chromophore concentration (1:0.23 stoichiometry) the first two SVs are comparable, and the transient accumulation of the P_r state in the time range of about 10 s is again clearly higher than at high chromophore concentration. The apparent dissociation constant K_D determined from the absorbance changes at 800 ms is 2.2 ± 0.5 μM. The time constants are comparable to those of full-length Cph1 and do not depend significantly on the protein:chromophore stoichiometry, except for the third relaxation associated with the photoconversion (see Table 1).

pH Dependence of the Assembly with PCB. Since the chromophore is protonated in P_r (*6*, *24*), whereas the free chromophore is unprotonated at neutral pH, protonation has to occur as part of the assembly process. To investigate the mechanism of this putative proton transfer, we studied the assembly at different pH values. Due to aggregation of the protein at lower pH and degradation of the free chromophore at high pH, we are restricted to a range from about pH 7 to pH 9.5. The results of the assembly at pH 8.7 are shown in Figure 7A−C. As at pH 7.9 (Figures 3−5) three relaxation steps are involved. The most obvious difference with the assembly at pH 7.9 is that the absorption spectrum at 800 ms after mixing (---) does not show the pronounced red-shifted absorption band at 680 nm and is closer to the spectrum at 10 ms (Figure 7A). Consequently, the amplitude of the first relaxation component is considerably smaller, as indicated by the time traces of the three relevant SVD components (Figure 7B) and the amplitude spectrum B_1 (■ in Figure 7C).

Experiments at pH 7 and 9.3 have been carried out in the same way. The results of the measurements at the different pH values are summarized in Table 2. To compare the amplitude of the first relaxation component, the difference spectrum $\Delta A = A$(800 ms) − A(10 ms) is shown at the four pH values in Figure 7D. The amplitude (ΔA at 680 nm) systematically decreases with increasing pH and nearly disappears at the highest value, suggesting that τ_1 is associated with proton transfer. This decrease is consistent with a pK_a of about 8.4, as indicated by a fit with the Henderson−Hasselbalch equation shown in the inset of Figure 7D.

The spectra at 23 s (···) and 200 s (− + −) reflecting the absorption changes of the third relaxation show that the transient accumulation of the P_r state after the second relaxation is lower at pH 8.7 than at pH 7.9 (Figure 7A). The changes in the second relaxation process are more evident from the time traces of the three relevant SVD components (Figure 7B). While the time constants of the first and the third relaxation ($\tau_1 = 130$ ms and $\tau_3 = 56$ s) are nearly unchanged, the time constant of the second relaxation is much larger ($\tau_2 = 11.5$ vs 2.5 s). Since the rise (τ_2) and decay (τ_3) times are closer together at higher pH, the related relaxations are not resolved in the trace of the first and dominating SVD component (Figure 7B), and the

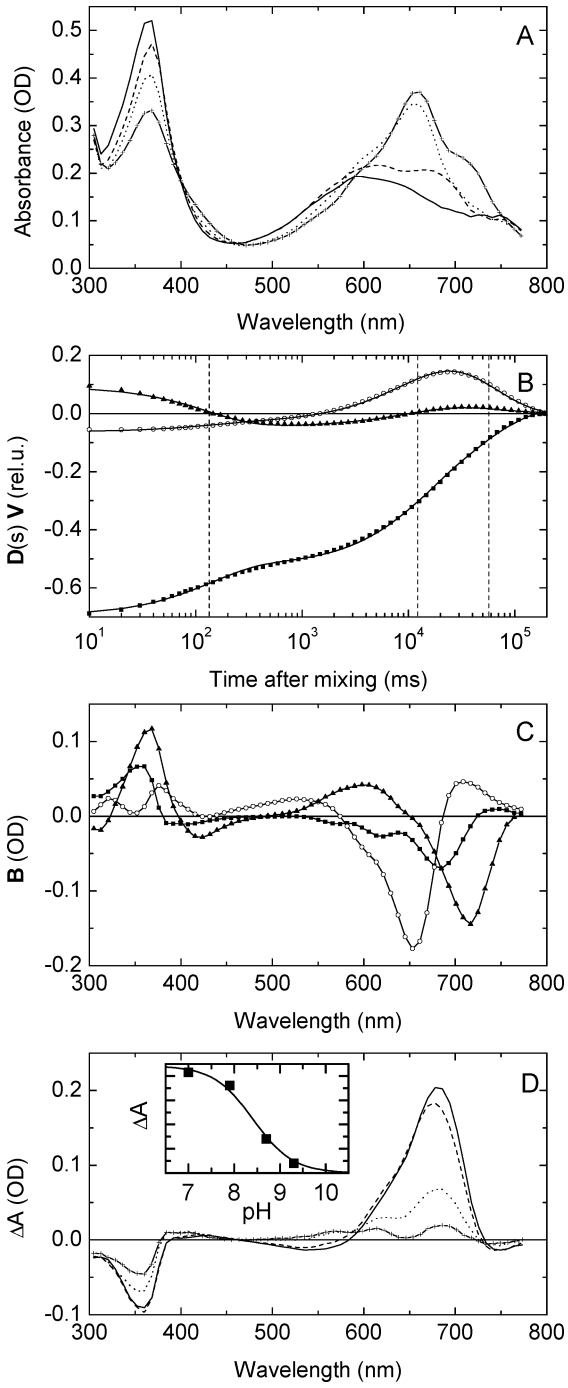

FIGURE 7: Stoichiometric assembly of apo-Cph1 with PCB at pH 8.7 and 10 °C in the time range from 10 ms to 200 s. (A) Absorption spectra at 10 ms (—), 800 ms (---), 23 s (···), and 200 s (— + —). (B) Time traces **D**(*s*)**V** of the main components of the SVD: s_1 = 3.400 (■), s_2 = 0.159 s_1 (○), and s_3 = 0.069 s_1 (▲). Solid lines represent a simultaneous fit to the data with three exponentials. Dashed vertical lines mark the time constants of the fit (τ_1 = 130 ms, τ_2 = 11 s, τ_3 = 56 s). (C) Amplitude spectra calculated from the fit amplitudes of panel B and the SVD basis spectra (data not shown): B_1 (■), B_2 (○), and B_3 (▲). (D) pH dependence of the difference spectra $\Delta A = A$(800 ms) − A(10 ms): pH 7.0 (—), pH 7.9 (---), pH 8.7 (···), and pH 9.3 (— + —); Inset: ΔA at 680 nm (■), fit to the data with a Henderson−Hasselbalch equation with a pK_a of 8.4 (—).

accumulation of the P_r state is lower. Accordingly, the contribution of the P_r decay in the amplitude spectrum B_3 is very small (Figure 7C).

Table 2: SVD and Kinetic Analysis of the Assembly of the Cph1 Apoprotein with PCB at Different pH Values

		singular values			time constants		
sample	pH	s_1	s_2/s_1	s_3/s_1	τ_1/ms	τ_2/s	τ_3/s
Cph1	7.0	1.948	0.441	0.162	168	2.7	56
	7.9	2.227	0.469	0.154	155	2.5	53
	8.7	3.400	0.159	0.069	134	11.5	56
	9.3	1.535	0.124	0.061	113	15.5	150

Noncovalent Assembly of IAA-Blocked Apoprotein with PCB. To identify the step associated with the covalent attachment of the chromophore, we investigated the assembly in samples of apoprotein in which the cysteine binding site is blocked by covalent reaction of the sulfhydryl group with IAA. The reaction was carried out as described (*22*). At an apoprotein concentration of 7 μM this reaction goes to completion at 1 mM IAA (*22*), as concluded from control experiments with 10 mM IAA. The noncovalent nature of the assembly complex was verified by the zinc fluorescence assay (*34*) and by the loss of PCB on a NAP-10 desalting column (Amersham-Pharmacia). The experiments were performed at 1:1 stoichiometry under identical conditions as before. The absorption spectra at 10 ms, 800 ms, and 200 s after mixing indicate that significant changes occur in the subsecond time range (Figure 8A). The scaled difference spectrum $\Delta A = A$(800 ms) − A(10 ms) is very similar to that of the nonblocked assembly under the same conditions (Figure 8B); i.e., a red-shifted intermediate is formed. Likewise, the kinetics in the subsecond time range are not affected by the IAA blocking, as shown by the scaled absorption changes at 680 nm (Figure 8C); i.e., $\tau_1 \approx 200$ ms.

Assembly with the Analogue PEB. The assembly with PEB, which can also form a covalent bond (see Figure 1), is comparable to that with PCB in the sense that transiently a red-shifted intermediate is formed. This is demonstrated in Figure 9A where the absorption spectra at 10 ms, 500 ms, and 200 s are shown. The SVD time traces were fitted with time constants of 65 ms, 3.3 s, and 190 s (Figure 9B), where the second component is nearly negligible. The related amplitude spectra are shown in Figure 9C: B_1 displays a negative amplitude at about 610 nm, reflecting the formation of the red-shifted intermediate, and B_3 displays a negative amplitude at 580 nm and a positive band at 610 nm, characterizing the transition from the red-shifted intermediate to the final (covalent) adduct. The formation of the covalent bond is thus almost 2 orders of magnitude slower than with PCB. A photoconversion component is absent since the PEB adduct is not photochromic.

CD Spectra of Cph1 with Covalently Bound PCB and PEB in P_r and P_{fr}. The CD spectrum of the P_r form was obtained after illumination with far-red light from a 3 mW light emitting diode emitting around 735 nm (Figure 10A). A CD spectrum of pure P_{fr} cannot be obtained directly, since the P_r/P_{fr} photoequilibrium is always below 70% P_{fr}. This spectrum was obtained by extrapolation from a set of CD spectra that were recorded during a "titration" of the sample with red light from a 1 mW diode laser emitting at 635 nm. In the course of this "light titration" by subsequent red irradiations the equilibrium between P_r and P_{fr} was successively shifted toward P_{fr} (65% in the photoequilibrium). For each value of the integrated illumination time, an absorption

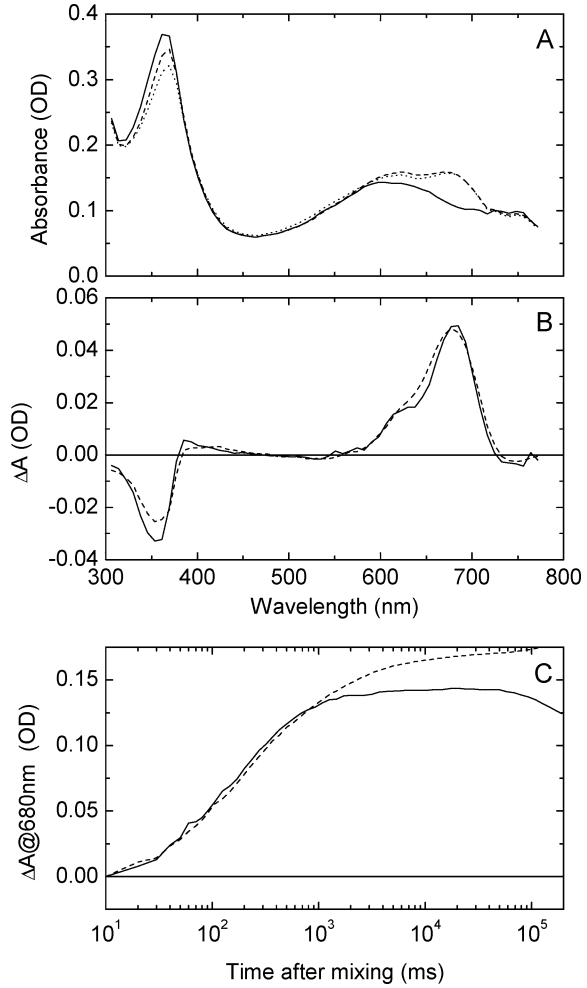

FIGURE 8: Assembly of IAA-blocked apo-Cph1 with PCB at pH 7.9 and 10 °C, stoichiometry 1:1, and apoprotein concentration 5.3 μM. (A) Absorption spectra at 10 ms (—), 800 ms (---), and 200 s (•••). (B) Difference spectra [A(800 ms) − A(10 ms)] blocked (—) and nonblocked (---). (C) Absorbance changes at 680 nm blocked (—) and nonblocked (---). Data of the blocked assembly in panels B and C are scaled by a factor of 2.5.

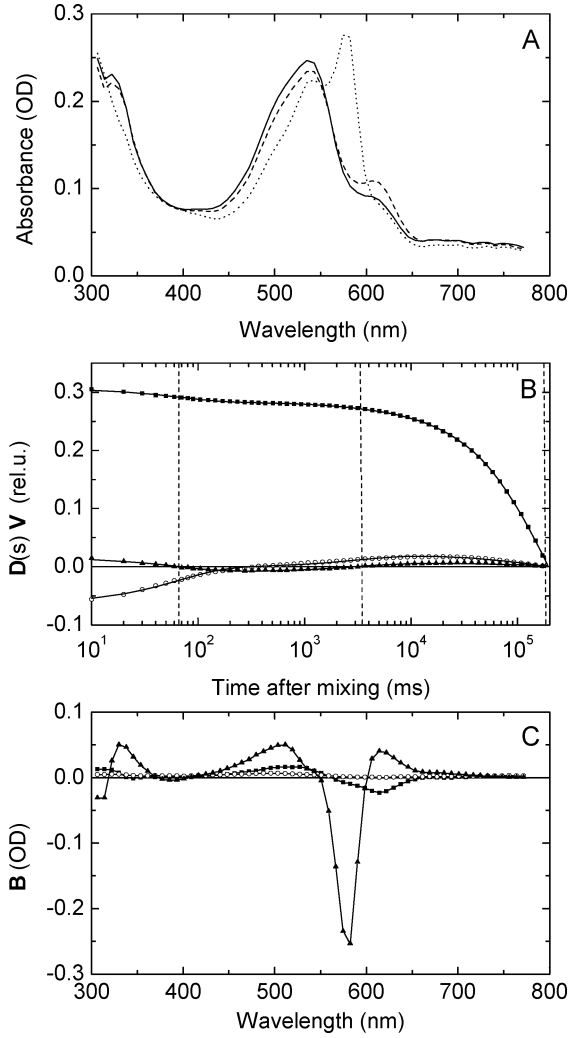

FIGURE 9: Assembly of apo-Cph1 with PEB at pH 7.9 and 10 °C, stoichiometry 1:1, and apoprotein concentration 6.3 μM. (A) Absorption spectra at 10 ms (—), 500 ms (---), and 200 s (•••). (B) Time traces **D**(s)**V** of the main components of the SVD: $s_1 = 1.928$ (■), $s_2 = 0.067\ s_1$ (○), and $s_3 = 0.020\ s_1$ (▲). Solid lines represent a simultaneous fit to the data with three exponentials. Dashed vertical lines mark the time constants of the fit ($\tau_1 = 65$ ms, $\tau_2 = 3.3$ s, $\tau_3 = 190$ s). (C) Amplitude spectra calculated from the fit amplitudes of panel B and the SVD basis spectra (data not shown): B_1 (■), B_2 (○), and B_3 (▲).

spectrum was taken before and after recording the CD spectrum using the CD cuvette. In this way we could exclude that photoconversion was induced by the measuring light of the CD spectrometer. From the combined set of absorption and CD spectra at nine values of the integrated red light intensity, the pure P_{fr} and P_r CD and absorption spectra were obtained by SVD analysis. The analysis confirmed the presence of only two species. The results for the CD spectra of pure P_r and P_{fr} are shown in Figure 10A. The P_r spectrum is characterized by a strong negative band centered at 640 nm and a strong positive band in the Soret range at 340 nm. In addition, there is a shoulder near 295 nm and a negative band around 265 nm. The P_{fr} spectrum, on the other hand, has a strong positive band centered around 675 nm and a negative band at 360 nm. The P_{fr} CD bands are red shifted with respect to the P_r bands, as expected from the corresponding shift in the absorption spectra. From the signs of the longest wavelength bands, one may conclude that in P_r and P_{fr} the chromophores have opposite chirality. The P_{fr} spectrum also has a positive band near 420 nm which is absent in the P_r spectrum. In addition, there is a negative band around 295 nm. The latter band may also be due to tyrosine and tryptophan residues of the apoprotein. To test this possibility and to gain a better understanding of the coupling between the electric transition dipole moments of these aromatic amino acids in the binding pocket and the transition dipoles of the chromophore, the CD spectra of the apoprotein and of apoprotein samples that were partially titrated with PCB were recorded. The apoprotein spectrum is shown in Figure 11A. From the titration results (data not shown), we concluded that the 295 nm band of P_{fr} and the 265 nm band of P_r are due to protein transitions. The large difference between the CD spectra of P_r and P_{fr} in the region below 420 nm indicates that the interactions between the chromophore and the aromatic amino acids in the binding pocket are quite different in P_r and P_{fr}.

Apo-Cph1 was also reconstituted with PEB, which lacks the C_{15}═C_{16} double bond between rings C and D. As a consequence the conjugated system is correspondingly

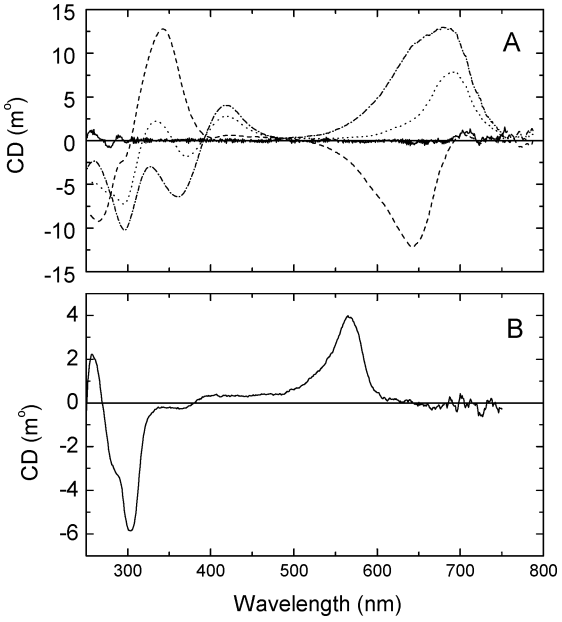

FIGURE 10: CD spectra of Cph1/bilin adducts and apo-Cph1. (A) PCB adduct: apo-Cph1 (—), P_r (---), P_r/P_{fr} photoequilibrium (•••), and P_{fr} (— • —); protein concentration = 12 μM. (B) PEB adduct; protein concentration = 6.5 μM.

shorter, leading to lower λ_{max} values. Since no photoisomerization can occur, only one dark state exists. The CD spectrum of Cph1/PEB is shown in Figure 10B. It is characterized by a narrow positive peak around 565 nm and a negative one near 305 nm. The major bands are blue shifted with respect to those of Cph1/PCB and centered at wavelengths expected from the absorption spectrum. Comparing with the Cph1/PCB spectra in Figure 10A, one concludes that the Cph1/PEB spectrum corresponds qualitatively with that of the P_{fr} state of Cph1/PCB.

Photoconversion and CD Spectra of Cph1 with Noncovalently Bound PCB. After the sulfhydryl group of cysteine 259, the chromophore binding site, was blocked with IAA, the labeled protein was incubated with PCB at a 1:1 stoichiomety. Illumination with red (635 nm) or far-red (750 nm) light led to a reversible photoconversion between "P_r-like" and "P_{fr}-like" states as shown in Figure 11A. For simplicity we will call these states P_r and P_{fr} in the following. Comparing Figure 11A with the corresponding results for the covalent adduct (Figure 2B or 4A), we note that the ratio of the absorbances in the visible and in the Soret bands is considerably smaller than for the case of covalent binding. Moreover, the ratio of the absorbances in the Q_x- and Q_y-bands in P_r is larger for the noncovalent complex. Both of these effects suggest the presence of a third spectral species, which is most likely due to PCB that is not bound in the binding pocket. Free or surface-bound PCB, for example, has a high absorbance in the Soret region and a broad lower absorbance near 600 nm, explaining our observations. Using the K_D value of 1.5 μM, determined for the noncovalent association in the absence of IAA, we may estimate from eq 7 that about 30% of the added PCB was unbound under the conditions of Figure 11A. This amount is of the right order of magnitude to explain the spectra in Figure 11A. Panel A of Figure 11 also shows the calculated spectrum of the pure P_{fr} state assuming that the P_r/P_{fr} photoequilibrium contains 50% P_r. This spectrum (•••) with Q_x- and Q_y-bands

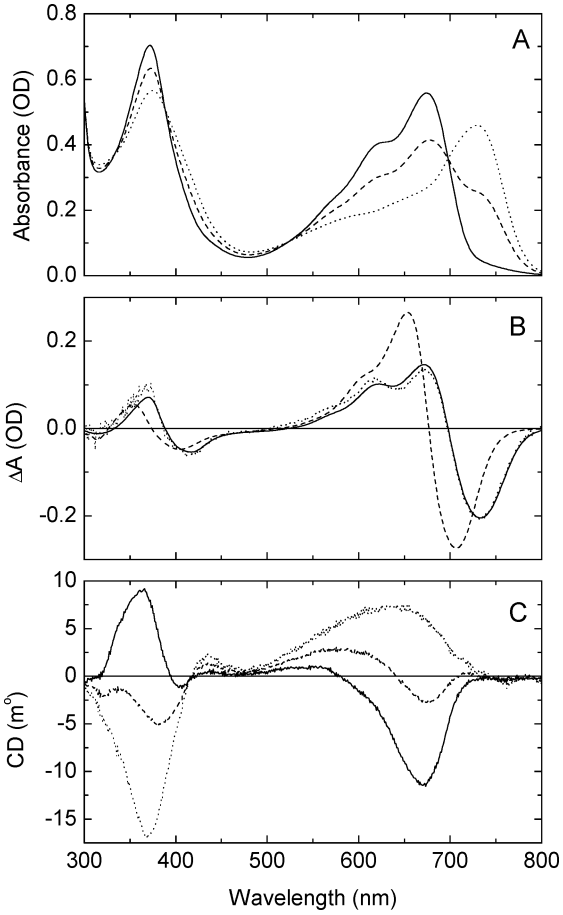

FIGURE 11: Spectral properties and photoconversion of noncovalent Cph1/PCB complexes, stoichiometry 1:1, and apoprotein concentration 14 μM. (A) Absorption spectra of the adduct assembled in the dark (—), after red illumination (---), and extrapolated for 100% P_{fr} (•••). (B) Difference spectra dark state minus red illuminated state: IAA-blocked PCB adduct (—), covalent PCB adduct scaled by a factor of 0.25 (---), and IAF-blocked PCB adduct (•••). (C) CD spectra of the IAA-blocked PCB adduct: after assembly in the dark (—), after red illumination (---), and extrapolated for 100% P_{fr} (•••).

looks like a canonical P_{fr} spectrum, except for the clear shoulder near 600 nm which is most likely due to the PCB that is not bound in the binding pocket. In panel B the P_r minus P_{fr} difference spectrum of the noncovalently bound PCB is compared with that of the covalent adduct. The absorption maximum and minimum of the noncovalently bound PCB are clearly red shifted by 25−30 nm with respect to covalently bound PCB. This is in agreement with the stopped-flow results where a red-shifted species was observed as the end product of the noncovalent assembly reaction (Figure 8A). We conclude that a covalent bond is not required for P_r/P_{fr} photochromicity.

We also blocked cysteine 259 with the much larger label iodoacetamidofluorescein (IAF), expecting that due to steric hindrance in the binding pocket, this blocking would prevent the noncovalent binding and photoconversion of PCB. Figure 11B shows, however, that even in the presence of IAF photoconversion between P_r- and P_{fr}-like Cph1/PCB states can take place. The P_r minus P_{fr} difference spectra for the IAA- and IAF-blocked samples are virtually identical (Figure 11B), suggesting similar chromophore geometries in the binding pocket.

The CD spectra of the P_r and P_{fr} states of IAA-blocked Cph1 with noncovalently bound PCB are shown in Figure 11C. The CD spectrum of P_r is similar to that for covalently bound PCB (Figure 10A), except for the following differences. (1) The negative rotational strength around 670 nm is red shifted with respect to the corresponding peak for covalently bound PCB (at about 640 nm). This is in accordance with the corresponding red shift in the absorbance difference spectrum (see Figure 11B). (2) The P_r spectrum contains an additional positive contribution between 500 and 580 nm. This positive rotational strength is probably an induced Cotton effect from PCB bound to the Cph1 surface (see Discussion). We may conclude that the conformation of the noncovalently bound PCB in the binding pocket in P_r is very similar to that of the covalently bound chromophore. The percentage photoconversion in the P_r/P_{fr} photoequilibrium was not determined directly. From the amplitude of the remaining negative band near 670 nm in the spectrum of the P_r/P_{fr} photoequilibrium in Figure 11C, we may estimate that the spectrum contains at least a 30% contribution from P_r. From simultaneous simulations of the absorption (Figure 11A) and CD (Figure 11C) spectra, we estimated that the P_r/P_{fr} photoequilibrium contains about 50% P_r. The corresponding calculated spectra for the pure P_{fr} states are plotted in panels A and C (···). The CD spectrum of the P_{fr} state in the visible is a superposition of two positive contributions from (1) surface-bound PCB centered near 580 nm (the same component that was detected in the absorption spectrum and that contributed to the CD spectrum of P_r) and (2) P_{fr} with a maximum near 650 nm. As for the covalent adduct (Figure 10A) the P_{fr} rotational strength in the longest wavelength band is positive. In contrast to the covalent adduct, however, where both Q_x and Q_y contribute (Figure 10A), almost all of the rotational strength comes from the Q_x transition. In the Soret band region the P_{fr} CD spectrum also has the signature of that of the covalent adduct, with a positive band near 430 nm and a larger negative band near 370 nm. So the signs and positions of these bands for P_{fr} are quite similar to those of the covalent adduct (410, 360 nm, Figure 10A) after correction for the red shift due to the extra double bond in the noncovalent adduct. The only significant qualitative difference between covalent and noncovalent adducts is the position of the longest wavelength CD band.

DISCUSSION

Mechanism and Kinetics of Self-Assembly. The improved time resolution of the stopped-flow method allowed us for the first time to resolve the formation of a red-shifted noncovalently bound intermediate in the self-assembly of Cph1/PCB and Cph1/PEB. The data (Figures 2B and 5A), and in particular the model-independent amplitude spectra B_1 (Figures 3D and 5D), show clearly that this intermediate with λ_{max} ~680 nm is formed in about 150−200 ms. The noncovalent character of this intermediate follows from the fact that when the reactive group of cysteine 259 is blocked with IAA, preventing the formation of the covalent bond with PCB, only this same red-shifted intermediate is formed with the same rise time (Figure 8). Moreover, the red shift with respect to the λ_{max} value of P_r at 655 nm is consistent with a noncovalent complex, since the conjugated system of the free chromophore is larger than for the covalent adduct due to the additional 3−3′ double bond. Further support for the origin of these spectral shifts comes from the photoconversion experiments with noncovalently bound PCB (Figure 11). In this case, the P_r minus P_{fr} difference spectrum was red shifted by about 25 nm with respect to the corresponding difference spectrum of the covalent adduct (Figure 11B).

On the basis of the B_2 amplitude spectra (Figure 3D), the second relaxation component is associated with a 25 nm blue shift, which is due to the loss of the 3−3′ double bond in the formation of the covalent bond in P_r. Whereas the related time constant (τ_2) ranges from 2.5 to 5 s for the natural chromophore PCB (see Table 1), it is about 200 s for the chromophore analogue PEB (Figure 9). The third relaxation component (in the assembly with PCB) is associated with photoconversion to P_{fr} by the measuring light. In the assembly experiments, the photoconversion was, however, always systematically slower than when preassembled holo-P_r was measured in the stopped-flow machine under identical conditions (e.g., 56 vs 25 s). The shape of the amplitude spectrum B_3 in Figure 3D and the time traces in Figure 4B indicate that the third relaxation step is not exclusively due to photoconversion but also contains significant contributions from a (slow) formation of (additional) P_r. We therefore conclude that the formation of the P_r state is biphasic, suggesting a P_r-like intermediate state (which is not photoconvertible) in a sequential pathway.

Variation of the molar apoprotein to PCB ratio in the range 1:0.3 to 1:4 had only a minor effect on the time constants τ_1 and τ_2 (Table 1) but had a major effect on the amplitude of the first component associated with the formation of the noncovalent complex (Figure 6). From the dependence of this amplitude on the PCB concentration we determined a value of 1.5 μM for the dissociation constant of this complex at 10 °C. This value is surprisingly close to the value of 1.3 μM at room temperature obtained in an entirely different way for the oat phytochrome A/PCB system (*12*). Its small value documents the strong noncovalent interaction with the binding pocket. With the mutant Cph1Δ2 we obtained a similar result for the dissociation constant (K_D = 2.2 μM), indicating that the histidine kinase domain does not affect the interaction of PCB with the binding pocket.

The pH could only be varied in the narrow range from 7 to 9.5. Table 2 shows that, in particular, τ_2 increases with pH. This leads to a reduction in the apparent amplitude of P_r since the formation time of P_r (τ_2) gets closer to its decay time τ_3. Of greater mechanistic interest is the observation that the amplitude of the red-shifted intermediate decreases strongly from pH 7 to pH 9.3 (Figure 7A,D). This supports the idea that PCB is protonated in this step. From these data a pK_a of 8.4 was obtained. From the fact that τ_1 is almost independent of pH (see Table 2), we may conclude that the protonation is intramolecular. The characteristic red shift and increase in oscillator strength of the Q-bands in the course of the formation of the red-shifted intermediate are probably due to a combination of (1) a transition to a more extended linear tetrapyrrole and (2) protonation of the chromophore. The chromophores in P_r and P_{fr} are known to be protonated (*6*, *10*, *24*), whereas the free chromophore is deprotonated at neutral pH. The pK_a of 8.4 may thus be interpreted as the pK_a of the proton donor in the apoprotein. Asp or Glu residues may have such high pK_a values in a hydrophobic environment. At high pH almost no red-shifted intermediate is found (Figure 7D), but P_r is still formed. This means that

protonation can apparently also occur by other slower pathways, e.g., directly from the external medium. We note that the pK_a of the chromophore deprotonation in P_r is 9.5 (*6*). The amplitude of P_r formation in the stopped-flow experiment at pH 9.3 was accordingly reduced.

Our results confirm and extend previous work on the kinetics of self-assembly in the phytochrome. A model involving a rapid preequilibrium with a noncovalent complex followed by formation of the covalent bond was proposed earlier (*16*) and partially confirmed (*12*). In these experiments only the formation of the final covalent adduct was observed and analyzed (*12*). Here we learn further aspects of the self-assembly mechanism from the concentration and pH dependence. Additional insight is obtained from experiments with blocked cysteine 259 and on a faster time scale than was previously accessible. The spectrum obtained at the earliest time point differs only slightly from free PCB (Figures 2B and 4A). We propose that this spectrum reflects the formation of a nonprotonated intermediate in which PCB is bound to the protein surface in a geometry comparable with that of free bilin in solution. Such an intermediate is moreover required for two reasons: (1) it explains the lack of concentration dependence of the time constant τ_1; (2) a rapid diffusion-controlled formation of a PCB−apoprotein complex is expected to be faster than the resolution of our stopped-flow apparatus. The second red-shifted noncovalent intermediate is then formed in about 150 ms. The associated spectral changes are due to stretching of the tetrapyrrole chain in the binding pocket and protonation. The overall K_D for this complex is 1.5 μM. The pK_a of the proton donor is 8.4. Indications for the existence of such red-shifted assembly intermediates were obtained for Cph1 from absorbance (*22*, *32*) and fluorescence (*35*) measurements and for *Calotrix* CphA from absorbance measurements (*23*), but their formation could not be time resolved. The stopped-flow method allowed for the first time to resolve the formation of this intermediate. Formation of P_r and the covalent bond is much slower with $\tau_2 \sim 2.5$ s.

How do our results compare with previous work in which only τ_2, the formation of the covalent bond, could be resolved? The most detailed investigation using a very sensitive fluorescence assay with recombinant oat phytochrome was performed in ref *12*. These authors exploited the high fluorescence quantum yield of bound PEB. The rates of the covalent reaction (τ_2) and dissociation constants for PΦB, PCB, and biliverdin were obtained indirectly from competitive inhibition experiments with PEB. It was not established in ref *12* whether the noncovalent complex with PEB was also fluorescent. Nevertheless, our values for τ_2 at 10 °C for Cph1 are in the same range as their values at room temperature for oat phy A: 2.5 and 4.0 s, respectively, for PCB and 200 and 20 s, respectively, for PEB. Further studies on the assembly kinetics were performed with plant phytochrome, all using absorption as the signal. In all cases the bilins were added in large excess, leading to pseudo-first-order conditions with exponential kinetics. This is in contrast to our experiments which were performed with molar apo/bilin ratios around 1. The observed values for τ_2 with PCB and PΦB varied between 9 and 500 s and were generally slower as obtained here for Cph1 (*13*, *14*, *16*, *20*, *21*). A plausible explanation for this apparent difference could be that the formation of the P_r state in plant phytochrome is also biphasic, as we concluded for Cph1 (see above). Due to insufficient time resolution only the late phase might have been observed, and thus the related time constant is rather comparable to time constant τ_3 in our experiments, which also includes a contribution from additional P_r formation (see Results section). For the bacteriophytochrome from *Calothrix* the assembly kinetics with PCB were studied with CphA, which forms a covalent adduct, and with CphB, in which a noncovalent complex is formed (*23*). As observed here, this noncovalent CphB/PCB complex showed P_r/P_{fr}-like photoconversion (*23*, *36*). At the position of the reactive cysteine in CphA, CphB has a leucine residue (*23*).

CD Spectroscopy of Cph1/PCB in P_r and P_{fr}: Isomerization Induces Chirality Reversal. CD spectroscopy is a more sensitive method to monitor the geometry of the chromophore and its interaction with the binding pocket than absorption spectroscopy. Extensive work has been done previously on the CD spectra of plant phytochrome (*37*−*41*). In plants PΦB is the natural chromophore which has one more double bond than PCB. For this reason absorption and CD spectra are red shifted by about 15−25 nm with respect to PCB adducts. Our spectrum for covalently bound PCB in the P_r form of Cph1 (Figure 10A) is in excellent qualitative agreement (signs of the major bands) with the main features of the plant phytochrome CD spectra in P_r, after correction for this red shift: a strong negative band in the visible (660−670 nm), a strong positive band in the Soret region (365−375 nm), and a negative band around 285 nm. The published CD spectra for the P_r/P_{fr} photoequilibrium of plants (typically 75−85% P_{fr}) are also in reasonable agreement (Figure 10A). The CD spectrum of the pure P_{fr} state for plant phytochromes has never been published but is generally considered to be "weaker", i.e., of lower amplitude, than that of P_r. The CD of the P_r/P_{fr} photoequilibrium shows besides a positive band around 720 nm a negative contribution from P_r at 665 nm. The positive 720 nm band is probably only apparently "weak" due to the overlap with the strong negative contribution at 665 nm from P_r. Such partial cancellations are well-known in CD spectroscopy. In the Soret region the positive peak around 360 nm is weaker in the photoequilibrium, and an additional positive band appears around 430 nm. Plant P_{fr} has also a negative band centered at 302 nm. From the reasonable agreement between the CD spectra of plants and Cph1 for both P_{fr} and P_r, we may conclude that the chromophore geometries in the respective binding pockets are also similar in both forms.

The extrapolation which allowed us to calculate CD spectra of pure P_{fr} showed for Cph1 that the longest wavelength band has positive rotational strength in P_{fr}. The chromophores in P_r and P_{fr} have thus opposite rotational strengths in this band. One way to interpret these results is to assign P_r and P_{fr} opposite chiralities (see below). The same probably holds for plant phytochromes. The experimental and theoretical aspects of the optical activity of free bilin and biliproteins have been investigated in detail (*37*, *38*, *42*, *43*). Bilins in solution assume a cyclic helical structure (*44*, *45*). In solution right- and left-handed helices with positive and negative rotational strengths in the longest wavelength band, respectively, are in equilibrium (*45*). Covalent binding to a cysteine in the binding pocket leads to extended rigid linear chromophores that are stabilized by interactions with the protein matrix. Such chromophore structures have been

extensively documented for a large number of biliproteins for which high-resolution X-ray structures are available (*25*−*29*). An exception is the bilin binding protein from *Pieris brassicae* (*46*). In this protein biliverdin IX γ is bound noncovalently in a cyclic right-handed helical structure. The ellipticity in the longest wavelength CD band of this protein is as expected positive and is in accord with the sign rule for C_2-symmetrical chromophores (*47*). On the basis of this structural calibration, we conclude that the positive and negative rotational strengths of P_{fr} and P_r correspond to right- and left-handed chromophore structures, respectively. The question that arises is how the isomerization around the C_{15}═C_{16} double bond between rings C and D leads to this change in chirality. One possibility is that the chromophore is right-handed in P_{fr} and that the large angular change of ring D induced by the isomerization leads to a net left-handed structure in P_r. Indeed, calculations show that when the first three rings are fixed in a left-handed arrangement, the rotational strength of the longest wavelength band could be either negative or positive depending on the values of the dihedral angles for the bridge between the third and fourth rings (*43*). It was concluded that "the calculated sign reversal of the CD bands can originate from rather small and localized conformational changes" (*43*). This simple picture for the origin of the chirality reversal from P_r to P_{fr} may be complicated by averaging effects from static or dynamic heterogeneity (substates). At least on the nanosecond time scale the chromophore is completely immobilized (*18*). In this connection it is of interest that in another photochromic biliprotein, phycoerythrocyanin from *Mastigocladus laminosus*, the longest wavelength CD band also reverses sign upon photoisomerization (*48*). As in phytochrome, 15 *Z*/*E* isomerization is involved, in this case with the chromophore phycoviolobilin (*48*). No explanation for this effect has been advanced so far.

CD Spectra of Cph1/PEB. From the CD spectrum of Cph1/PEB (Figure 10B) we may conclude by comparison with Figure 10A that this nonisomerizable chromophore has a CD spectrum similar to that of PCB in the P_{fr} state. The positive CD in the longest wavelength band of the PEB adduct may be rationalized by assuming the same right-handed structure for the first three rings as in the PCB, as dictated by similar interactions with the binding pocket. Since ring D of PEB is not part of the conjugated system, it does not contribute to the CD. We note that the PEB chromophore is indeed rigidly held in the binding pocket, as was shown by time-dependent fluorescence depolarization measurements (*18*). Since Cph1 is a homodimer, chromophore−chromophore interactions could lead to exciton effects in the CD spectra. Fluorescence energy transfer experiments with PEB−Cph1 suggest, however, that the interchromophore distance is 56 $\pm$ 7 Å (*18*). In accordance with the experimental CD spectra, this is too far for CD exciton effects.

Photoconversion of Noncovalently Bound PCB. After blocking the cysteine binding site with IAA, noncovalent binding of PCB still occurred (Figures 8 and 11). Moreover, we showed from both absorption and CD measurements that photoconversion between P_r- and P_{fr}-like states does not require the covalent linkage with cysteine 259 (Figure 11). Both the absorption and CD spectra of the noncovalently bound PCB were red shifted by about 25 nm with respect to their values for covalently bound PCB (see, e.g., Figure 11B). The most likely explanation for this red shift is that the conjugated system is larger for the noncovalently bound chromophore than for the covalent adduct, since the 3−3′ double bond to ring A is lost upon formation of the covalent linkage. The experiments thus provide a plausible explanation for the red-shifted intermediates observed in the stopped-flow experiments with PCB and PEB (τ_1) and for the red-shifted end product in the stopped-flow experiment with Cph1/IAA/PCB. They explain, moreover, the blue shift of about 25 nm in the τ_2 component of the Cph1/PCB stopped-flow experiment, which is associated with the formation of the covalent bond.

The similarity between the CD spectra of covalently and noncovalently bound PCB in P_r strongly suggests an analogous chromophore geometry in the binding pocket. For the P_{fr} form the CD data also indicate great structural similarity for the covalently and noncovalently bound chromophores. The data of Figure 11A,B show that the covalent anchoring of ring A by cysteine 259 is not required for photochromism. The structural explanation for this surprising observation is provided by the CD results. They show that the chromophores are already in the appropriate geometry in the absence of the covalent bond. Noncovalent interactions with the binding pocket, such as the salt bridge between rings B and C and an acidic counterion and the anchoring by the propionate side chains, are apparently sufficient to keep the chromophore in the proper geometry for isomerization.

In the absorption spectra of noncovalently bound PCB we detected the presence of a population of nonphotochromic PCB with spectral characteristics similar to those of free PCB, suggesting that these molecules are not in the binding pocket. As the first unresolved intermediate in the stopped-flow experiments we also detected such a spectral component (Figure 2B), which may well be due to surface-bound PCB. In the CD spectra (Figure 11C) this species contributed the broad positive bands centered near 580 nm in P_r and P_{fr}. PCB is amphiphilic and may well bind to the protein surface. It is well-known that other linear tetrapyrroles like bilirubin and biliverdin strongly bind to bovine and human serum albumin, leading to large induced CD effects (*42*, *49*).

Blocking cysteine 259 with the bulky chromophore IAF surprisingly still allowed light-induced photoconversion of the noncovalently bound PCB. The light-induced difference spectrum was virtually identical to that of IAA-blocked Cph1 (Figure 11B). Similar results were obtained with even larger blocking groups such as Texas Red (data not shown). These remarkable results are difficult to explain with a model in which cysteine 259 is deeply buried in the protein at the end of an elongated binding pocket. Steric hindrance would then be expected to prevent the proper interactions of the chromophore with the binding pocket. If the reactive sulfhydryl of cysteine 259 were near the protein surface, however, the bound fluorescein or Texas Red might project into the aqueous solution, thereby leaving the binding pocket entrance open and the binding pocket unoccupied. In this model ring A would be near the surface, and ring D could be deeply buried. Since the photoisomerization switch involves ring D, this position for ring D would be quite appropriate for the coupling of the changed chromophore geometry to the protein.

CONCLUSION

The combined kinetic and spectroscopic evidence suggests the following reaction scheme for the bilin self-assembly in Cph1 of *Synechocystis*:

$$\mathrm{bi} + \mathrm{apoH}^+ \rightleftharpoons \mathrm{bi{\cdot}apoH}^+ \underset{\tau_1}{\rightleftharpoons} \mathrm{bi\ H}^+{\cdot}\mathrm{apo} \underset{\tau_2}{\rightarrow} \mathrm{holoP_r} \underset{\tau_3}{\rightleftharpoons} \mathrm{holoP_{fr}}$$

bi·apoH$^+$ is the first noncovalent intermediate, and bi H$^+$· apo is the second red-shifted noncovalent intermediate. In τ_1 the chromophore is protonated by intramolecular proton transfer. For PCB, the time constants are $\tau_1 \sim 150$ ms, $\tau_2 \sim 2.5$ s, and $\tau_3 \sim 50$ s. The K_D for the noncovalent complex is $\sim$1.5 μM.

Reversible photoconversion between P_r- and P_{fr}-like states occurs in Cph1 even in the absence of a covalent bond. The CD spectra of the noncovalent complex suggest that the noncovalent interactions in the binding pocket are sufficient to keep the linear tetrapyrrole in the appropriate geometry for photoisomerization.

ACKNOWLEDGMENT

We thank Connie Goerick, Ines Heiland, Stefanie Krohn, and Norbert Michael for preparation and purification of apo-Cph1, PCB, and PEB and our physics students Oliver Penz and Dirk Opitz for developing the control and data acquisition systems for the stopped-flow and CD spectropolarimeter, respectively.

REFERENCES

1. Kendrick, R. E., and Kronenberg, G. H. M., Eds. (1994) *Photomorphogenesis in Plants*, 2nd ed., Kluwer Academic Publishers, Dordrecht, The Netherlands.
2. Sineshchekov, V. A. (1995) *Biochim. Biophys. Acta 1228*, 125−164.
3. Montgomery, B. L., and Lagarias, J. C. (2002) *Trends Plant Sci. 7*, 357−366.
4. Yeh, K.-C., Wu, S.-H., Murphy, J. T., and Lagarias, J. C. (1997) *Science 277*, 1505−1508.
5. Remberg, A., Lindner, I., Lamparter, T., Hughes, J., Kneip, K., Hildebrandt, P., Braslavsky, S. E., Gärtner W., and Schaffner, K. (1997) *Biochemistry 36*, 13389−13395.
6. van Thor, J. J., Borucki, B., Crielaard, W., Otto, H., Lamparter, T., Hughes, J., Hellingwerf, K. J., and Heyn, M. P. (2001) *Biochemistry 40*, 11460−11471.
7. Andel, F., III, Murphy, J. T., Haas, J. A., McDowell, M. T., van der Hoef, I., Lugtenburg, J., Lagarias, J. C., and Mathies, R. A. (2000) *Biochemistry 39*, 2667−2676.
8. Foerstendorf, H., Benda, C., Gärtner, W., Storf, M., Scheer, H., and Siebert, F. (2001) *Biochemistry 40*, 14952−14959.
9. Andel, F., III, Lagarias, J. C., and Mathies, R. A. (1996) *Biochemistry 35*, 15997−16008.
10. Kneip, C., Hildebrandt, P., Schlamann, W., Braslavsky, S. E., Mark, F., and Schaffner, K. (1999) *Biochemistry 38*, 15185−15192.
11. Lagarias, J. C., and Lagarias, D. M. (1989) *Proc. Natl. Acad. Sci. U.S.A. 86*, 5778−5780.
12. Li, L., Murphy, J. T., and Lagarias, J. C. (1995) *Biochemistry 34*, 7923−7930.
13. Deforce, L., Furuya, M., and Song, P. S. (1993) *Biochemistry 32*, 14185−14172.
14. Remberg, A., Schmidt, P., Braslavsky, S. E., Gärtner, W., and Schaffner, K. (1999) *Eur. J. Biochem. 266*, 201−208.
15. Wu, S.-H., and Lagarias, J. C. (2000) *Biochemistry 39*, 13487−13495.
16. Li, L., and Lagarias, J. C. (1992) *J. Biol. Chem. 267*, 19204−19210.
17. Bhoo, S. H., Hirano, T., Jeong, H.-Y., Lee, J.-G., Furuya, M., and Song, P.-S. (1997) *J. Am. Chem. Soc. 119*, 11717−11718.
18. Otto, H., Lamparter, T., Borucki, B., Hughes, J., and Heyn, M. P. (2003) *Biochemistry 42*, 5885−5895.
19. Nagasako, M., Wada, M., Tokutomi, S., Yamamoto, K. T., Sakai, J., Kataoka, M., Tokunaga, F., and Furuya, M. (1990) *Photochem. Photobiol. 52*, 3−12.
20. Remberg, A., Ruddat, A., Braslavsky, S. E., Gärtner, W., and Schaffner, K. (1998) *Biochemistry 37*, 9983−9990.
21. Kunkel, T., Tomizawa, K.-I., Kern, R., Furuya, M., Chua, N.-H., and Schäfer, E. (1993) *Eur. J. Biochem. 215*, 587−594.
22. Lamparter, T., Esteban, B., and Hughes, J. (2001) *Eur. J. Biochem. 268*, 4720−4730.
23. Jorissen, H. J. M. M., Quest, B., Remberg, A., Coursin, T., Braslavsky, S. E., Schaffner, K., Tandeau de Marsac, N., and Gärtner, W. (2002) *Eur. J. Biochem. 269*, 2662−2671.
24. Foerstendorf, H., Lamparter, T., Hughes, J., Gärtner, W., and Siebert, F. (2000) *Photochem. Photobiol. 71*, 655−661.
25. Schirmer, T., Bode, W., and Huber, R. (1987) *J. Mol. Biol. 196*, 677−695.
26. Brejc, K., Ficner, R., Huber, R., and Steinbacher, S. (1995) *J. Mol. Biol. 249*, 424−440.
27. Duerring, M., Huber, R., Bode, W., Ruembeli, R., and Zuber. H. (1990) *J. Mol. Biol. 211*, 633−644.
28. Ficner, R., Lobeck, K., Schmidt, G., and Huber, R. (1992) *J. Mol. Biol. 228*, 935−950.
29. Chang, W. R., Jiang, T., Wan, Z. L., Zhang, J. P., Yang, Z. X., and Liang, D. C. (1996) *J. Mol. Biol. 262*, 721−731.
30. Stanek, M., and Grubmayr, K. (1996) *Chem. Eur. J. 4*, 1653−1659.
31. Hughes, J., Lamparter, T., Mittmann, F., Hartmann, E., Gärtner, W., Wilde, A., and Börner, T. (1997) *Nature 386*, 663−663.
32. Lamparter, T., Mittmann, F., Gärtner, W., Börner, T., Hartmann, E., and Hughes, J. (1997) *Proc. Natl. Acad. Sci. U.S.A. 94*, 11792−11797.
33. Hübschmann, T., Börner, T., Hartmann, E., and Lamparter, T. (2001) *Eur. J. Biochem. 268*, 2055−2063.
34. Berkelman, T. R., and Lagarias, J. C. (1986) *Anal. Biochem. 156*, 194−201.
35. Sineshchekov, V. A., Koppel, L., Esteban, B., Hughes, J., and Lamparter, T. (2002) *J. Photochem. Photobiol. B 67*, 39−50.
36. Jorissen, H. J. M. M., Quest, B., Lindner, I., Tandeau de Marsac, N., and Gärtner, W. (2002) *Photochem. Photobiol. 75*, 554−559.
37. Björling, S. C., Zhang, C.-F., Farrens, D. L., Song, P.-S., and Kliger, D. S. (1992) *J. Am. Chem. Soc. 114*, 4581−4588.
38. Song, P.-S., Chae, Q., and Gardner, J. D. (1979) *Biochim. Biophys. Acta 576*, 479−495.
39. Vierstra, R. D., Quail, P. H., Hahn, T.-R., and Song, P.-S. (1987) *Photochem. Photobiol. 45*, 429−432.
40. Litts, J. C., Kelly, J. M., and Lagarias, J. C. (1983) *J. Biol. Chem. 258*, 11025−11031.
41. Brandlmeier, T., Lehner, H., and Rüdiger, W. (1981) *Photochem. Photobiol. 34*, 69−73.
42. Wagnière, G., and Blauer, G. (1976) *J. Am. Chem. Soc. 98*, 7806−7810.
43. Scharnagl, C., Köst-Reyes, E., Schneider, S., Köst, H.-P., and Scheer, H. (1983) *Z. Naturforsch. 38c*, 951−959.
44. Falk, H. (1989) *The Chemistry of Linear Oligopyrroles and Bile Pigments*, Springer-Verlag, Berlin and New York.
45. Knipp, B., Müller, M., Metzler-Nolte, N., Baladan, T. S., Braslavsky, S. E., and Schaffner, K. (1998) *Helv. Chim. Acta 81*, 881−888.
46. Huber, R., Schneider, M., Mayr, I., Müller, R., Deutzmann, R., Suter, F., Zuber, H., Falk, H., and Kayser, H. (1987) *J. Mol. Biol. 198*, 499−513.
47. Hug, W., and Wagnière, G. (1972) *Tetrahedron 28*, 1241−1248.
48. Zhao, K.-H., and Scheer, H. (1995) *Biochim. Biophys. Acta 1228*, 244−253.
49. Blauer, G., and Wagnière, G. (1975) *J. Am. Chem. Soc. 97*, 1949−1954.

BI035511N